Characterization of Concurrent Dual-band Power Amplifiers Using a Dual Two-tone Excitation Signal

Shoaib Amin, *Student Member, IEEE,* Wendy Van Moer, *Senior Member, IEEE,* Peter Händel, *Senior Member, IEEE,* and Daniel Rönnow, *Member, IEEE*

***Abstract*—A method to characterize the memory effects in a nonlinear concurrent dual-band transmitter is presented. It is an extension of the conventional two tone test for power amplifiers to concurrent dual band transmitters. The output signal of a concurrent dual-band transmitter is affected not only by intermodulation products but also by cross-modulation products. In one frequency band, the transmitter is excited by a two tone signal which frequency separation is swept. In the second band the transmitter is concurrently excited by an other two tone signal with slightly wider frequency separation. The frequency difference of the two signals is fixed during the frequency sweep. The two tone test is made at different power levels. The upper and lower third-order inter- and cross-modulation products are measured. The asymmetry between the upper and lower third-order inter- and cross-modulation products are measures of the transmitter's memory effects. The measurement results show that the memory effects are more dominant in the third-order intermodulation products than in the cross modulation products. An error analysis and system calibration was performed and measurement results for two different devices are presented.**

***Index Terms*—Amplifier distortion, concurrent dual-band, power amplifier, intermodulation, cross-modulation, multiple-input multiple-output (MIMO), digital pre-distortion.**

I. Introduction

During a two-tone test of radio frequency (RF) and microwave amplifiers, the amplitude and in some cases the phase of the third-order intermodulation (IM) products in the pass-band around the carrier frequency are measured and used as a measure of nonlinearity. Metrics, like the third-order intercept point can be derived from the measured IM products [1].

Frequency dependence and the asymmetry of upper and lower IM products versus tone spacing (frequency spacing) is used as a qualitative measure of memory effects in the nonlinear transfer function of a device [2]–[6]. Sweeping the amplitude of the two input tones and measuring the amplitude of the IM products can be used to identify sweet spots and transitions between the small and large signal regimes of a device [7].

The IM products at a specific tone spacing are due to all odd nonlinear orders (third, fifth, seventh, $\cdots$). The measured IM products are therefore the combination of all contributions from these nonlinear orders. The third-order Volterra kernel (nonlinear transfer function) is a function of three frequencies and requires three input tones to be characterized in the general case. The correct determination also requires that the higher order contributions (fifth, seventh, ...) are compensated for [8].

Early two-tone tests used different local oscillators for the two tones and only the IM amplitude could be measured [9], [10]. Methods to measure the IM phase by using reference nonlinear devices were developed later [11], [12]. IM amplitude and phase were measured without a phase reference by up-converting a modulated signal (the two-tone signal) to RF [2], [13], [14].

In recent years, there has been an increased interest in RF devices with multiple input and output channels. One example is the concurrent dual-band RF amplifier that operates with two modulated input and two output signals at different center frequencies concurrently and the difference between the operational carrier frequencies is hundreds of MHz to GHz [15]–[17]. Another example is multiple-input multiple-output (MIMO) transmitters in which cross-talk between the channels make them nonlinear MIMO systems in practice [18]–[20] (i.e., not multiple SISO systems). The latter application is of importance in massive MIMO applications. In [15], a two-tone test of a concurrent dual-band RF amplifier was reported, but no amplitude or frequency sweeps were performed. In [16], a two two-tone test was reported where the characterization of memory effect was performed by sweeping the frequency of one of the two two-tone signals operating in one band while keeping the frequency spacing of the other signal operating in the other band fixed. The Volterra kernels were excited like in some three-tone test in [8], rather than as in conventional two-tone tests where the kernels are excited along their diagonal [8].

In this paper, we present a method for the characterization of memory effects in a concurrent dual-band transmitter, where the characterization is performed by injecting a two-tone test signal in each input channel of the transmitter, while sweeping both the power and frequency of both signals. The proposed method is similar to a conventional two-tone test for SISO transmitter, where the power and frequency of the two-tone signal are swept [2]. The Volterra kernels are excited along paths similar to those of a conventional two-tone test [8]. The

Shoaib Amin is with the Department of Electronics, Mathematics and Natural Sciences, University of Gävle, SE-80176, Gävle, Sweden, and also with the Department of Signal Processing, ACCESS Linnaeus Centre, KTH Royal Institute of Technology, SE-10044 Stockholm e-mail: (shoaib.amin@hig.se).

Wendy van Moer is with the Department of Electronics, Mathematics and Natural Sciences University of Gävle, SE-80176, Gävle, Sweden email: (Wendy.Van.Moer@hig.se).

Peter Händel is with the Department of Signal Processing, ACCESS Linnaeus Centre, KTH Royal Institute of Technology, SE-10044 Stockholm and also with the Department of Electronics, Mathematics and Natural Sciences University of Gävle, SE-80176, Gävle, Sweden email: (ph@kth.se).

Daniel Rönnow is with the Department of Electronics, Mathematics and Natural Sciences University of Gävle, SE-80176, Gävle, Sweden email: (daniel.ronnow@hig.se).

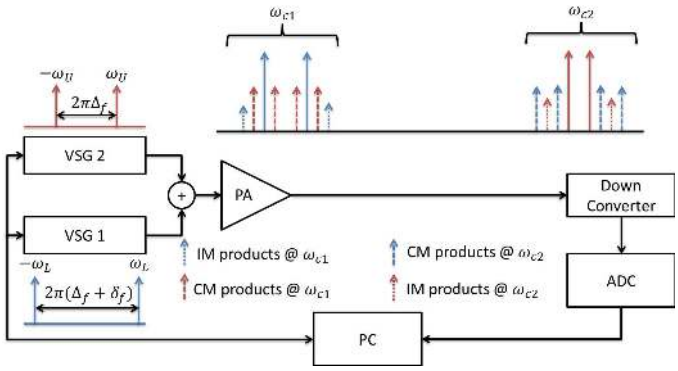

Fig. 1. Measurement setup for the characterization of concurrent dual-band power amplifier. $\pm\omega_L$ and $\pm\omega_U$ are the frequencies of two two-tone signals relative to carrier frequencies ω_{c1} and ω_{c2}, respectively.

method can be easily adapted for MIMO transmitters. The important difference with the conventional two-tone test is that the baseband and the RF coherency between two test signals have to be considered in the error analysis. Moreover, the proposed method could also be used before the implementation of a digital pre-distortion (DPD) algorithm for the linearization of a multi-band transmitter, but this has not been investigated in this paper. Since the method characterizes the memory effects appearing in the IM and cross-modulation (CM) products, this information could be utilized for the optimization of DPD models (i.e., parametric memory polynomial models) in terms of memory depth and nonlinear order.

In Section II, a general framework is developed to study the IM and CM effects appearing in a concurrent dual-band transmitter. Additionally, an approach for evaluating these modulation effects has been developed. The experimental setup is presented in Section III. The measurement results are presented and analyzed in Section IV.

II. Theory

When a nonlinear device is excited by a multiple frequency signal centered around a carrier and driven in its nonlinear region, it generates mixing products. These mixing products are generated near the excited frequencies, at the baseband and at the harmonics of the fundamental frequencies. Mixing products that appear close to the fundamental frequencies are of interest, since they cannot be filtered out and, thus, need to be characterized. Compensation should be made in terms of linearization, either digitally or through hardware.

In a dual-band transmitter, Fig. 1, the mixing products due to nonlinearity will cause not only IM products, but also CM products. These CM products, in general, occur because of the nonlinear interaction of the signals operating at different carrier frequencies. In the following section, a mathematical derivation of the presence of CM products and their frequency location is shown.

A. Distortion in a Dual-band Transmitter

The output signal of a static nonlinear device such as a power amplifier (PA) is conventionally represented by a power series of the input signal and can be written as

$$y_{out}(t) = h_1 x_{in}(t) + h_2 x_{in}^2(t) + h_3 x_{in}^3(t) + \ldots, \quad (1)$$

where $h_1 - h_3$ are real-valued coefficients; below we will also introduce dynamic effects (memory effects). In (1), $x_{in}(t)$ and $y_{out}(t)$ are the time domain input and output signals, respectively. When studying the nonlinear behavior of a device, the signal contributions close to the carrier frequency are of interest. The even order terms of the power series are filtered, since they do not contribute to the equivalent baseband model in the fundamental frequency zone [21]. For a dual-band transmitter, the input signal $x_{in}(t)$ can be written as,

$$x_{in}(t) = Re\{\,\alpha_1(t)e^{j\omega_{c_1}t}\,\} + Re\{\,\alpha_2(t)e^{j\omega_{c_2}t}\,\}, \quad (2)$$

where $\alpha_1(t)$, $\alpha_2(t)$ are the complex envelope input signals for each band and ω_{c_1}, ω_{c_2} are the carrier frequencies, respectively. If $\alpha_1(t)$ and $\alpha_2(t)$ are the two two-tone signals, then x_{in} can be written as

$$x_{in}(t) = A_1\cos(\omega_L t)\cos(\omega_{c_1}t + \varphi_L) + A_2\cos(\omega_U t)\cos(\omega_{c_2}t + \varphi_U),$$

where A_1, A_2 are the amplitudes, ω_L, ω_U are the frequencies of the two two-tones relative to the carrier frequencies ω_{c1} and ω_{c2}, respectively, as illustrated in Fig. 2 and φ_L, φ_U are the phases of respective two two-tone signals. Assume that the two two-tone signals have the same amplitude and $\varphi_L = \varphi_U = 0$, the resulting input signal x_{in} can be written as,

$$x_{in}(t) = A\left[\cos(\omega_L t)\cos(\omega_{c_1}t) + \cos(\omega_U t)\cos(\omega_{c_2}t)\right]. \quad (3)$$

Inserting (3) in (1) and assuming PA to be weakly nonlinear, thus restricting (1) to third-order nonlinearities. The output of a dual-band transmitter can be described as

$$\begin{aligned} y_{out}(t) &= Ah_1\{[\cos(\omega_L t)\cos(\omega_{c_1}t) + \cos(\omega_U t)\cos(\omega_{c_2}t)]\} \\ &\quad + A^3h_3\{[\cos(\omega_L t)\cos(\omega_{c_1}t) + \cos(\omega_U t)\cos(\omega_{c_2}t)]\}^3 \\ &= Ah_1\{[\cos(\omega_L t)\cos(\omega_{c_1}t) + \cos(\omega_U t)\cos(\omega_{c_2}t)]\} \\ &\quad + A^3h_3\Bigg\{\underbrace{[\cos^3(\omega_L t)\cos^3(\omega_{c_1}t)}_{\text{a}} + \underbrace{\cos^3(\omega_U t)\cos^3(\omega_{c_2}t)]}_{\text{b}} \\ &\quad + \underbrace{3\cos^2(\omega_L t)\cos^2(\omega_{c_1}t)\cos(\omega_U t)\cos(\omega_{c_2}t)}_{\text{c}} \\ &\quad + \underbrace{3\cos^2(\omega_U t)\cos^2(\omega_{c_2}t)\cos(\omega_L t)\cos(\omega_{c_1}t)}_{\text{d}}\Bigg\}. \end{aligned} \quad (4)$$

Eqn. (4) shows the linear and higher order response of a system to a dual-band input signal $x_{in}(t)$. By using trigonometric properties on the terms a, b, c and d (see Appendix), the dual-band output signal $y_{out}(t)$ can be written as

$$y_{\omega_L}(t) = \Bigg[\underbrace{(Ah_1 + \frac{21A^3h_3}{16})\cos(\omega_L t)}_{\text{fundamental tones @ } \omega_{c_1}} + \underbrace{(\frac{3A^3h_3}{16})\cos(3\omega_L t)}_{\text{IM @ } \omega_{c_1}} \quad (5)$$

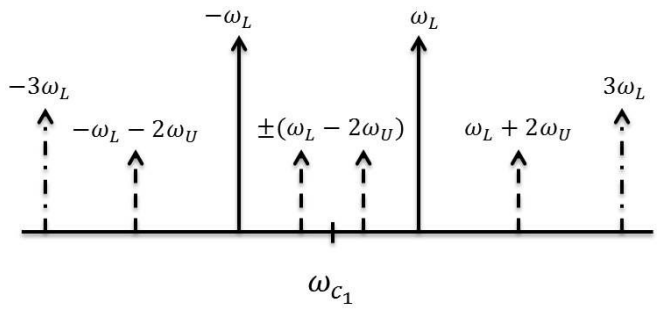

Fig. 2. Illustration of the frequency location of IM and CM products derived in equation (7)

$$+\underbrace{(\frac{3A^3h_3}{4})\cos(\omega_L t)\cos(2\omega_U t)}_{\text{CM @ } \omega_{c_1}}\Bigg]\cos(\omega_{c_1}t),$$

$$y_{\omega_U}(t) = \Bigg[\underbrace{(Ah_1 + \frac{21A^3h_3}{16})\cos(\omega_U t)}_{\text{fundamental tones @ } \omega_{c_2}} + \underbrace{(\frac{3A^3h_3}{16})\cos(3\omega_U t)}_{\text{IM @ } \omega_{c_2}} \tag{6}$$

$$+\underbrace{(\frac{3A^3h_3}{4})\cos(\omega_U t)\cos(2\omega_L t)}_{\text{CM @ } \omega_{c_2}}\Bigg]\cos(\omega_{c_2}t),$$

where $y_{\omega_L}(t)$, $y_{\omega_U}(t)$ are the two output signals at carrier frequencies ω_{c_1} and ω_{c_2}, respectively.

Using complex exponentials and introducing separate coefficients for each frequency component, the lower band output signal $y_{\omega_L}(t)$ in (5) can be re-written as

$$y_{\omega_L}(t) = \Bigg[\frac{A}{2}(h_1^{(+)}e^{j\omega_L t} + h_1^{(-)}e^{-j\omega_L t}) + \tag{7a}$$

$$\frac{21A^3}{32}(h_{3_{IM}}^{(+)}e^{j\omega_L t} + h_{3_{IM}}^{(-)}e^{-j\omega_L t}) + \tag{7b}$$

$$(\frac{3A^3}{32})\underbrace{(h_{3_{IM}}^{(+)}e^{j3\omega_L t} + h_{3_{IM}}^{(-)}e^{-j3\omega_L t})}_{\text{IM products @ } \omega_{c_1}} + \tag{7c}$$

$$(\frac{3A^3}{16})\underbrace{(h_{3_{CM_{Out}}}^{(+)}e^{j(\omega_L+2\omega_U)t} + h_{3_{CM_{Out}}}^{(-)}e^{-j(\omega_L+2\omega_U)t})}_{\text{Outer CM products @ } \omega_{c_1}} + \tag{7d}$$

$$(\frac{3A^3}{16})\underbrace{(h_{3_{CM_{In}}}^{(+)}e^{j(\omega_L-2\omega_U)t} + h_{3_{CM_{In}}}^{(-)}e^{-j(\omega_L-2\omega_U)t})}_{\text{Inner CM products @ } \omega_{c_1}}\Bigg]e^{j(\omega_{c_1}t)}, \tag{7e}$$

where in (7), $h_1^{(+)}$, $h_1^{(-)}$ are the coefficients of the frequency components at $\omega_{c_1} + \omega_L$ and $\omega_{c_1} - \omega_L$, respectively. Similarly, $h_{3_{IM}}^{(+)}$, $h_{3_{IM}}^{(-)}$ are the coefficients of upper and lower IM products, respectively. In (7), $h_{3_{CM_{Out}}}^{(+)}$, $h_{3_{CM_{Out}}}^{(-)}$ are the coefficients of upper and lower outer CM products and $h_{3_{CM_{In}}}^{(+)}$, $h_{3_{CM_{In}}}^{(-)}$ are the coefficients of upper and lower inner CM products. In Table I, the corresponding frequency domain Volterra kernels (frequency domain nonlinear transfer functions) for the coefficients in (7) are given. Note that the frequency domain Volterra kernels of the IM products (e.g., row 5 in Table I) are different from the frequency domain Volterra kernels of the CM products (e.g., row 8 in Table I), this is also indicated in $(7a - e)$ where each frequency component has different coefficient.

In (7), the lower band output signal $y_{\omega_L}(t)$ has terms dependent on both input signals, where (7c) indicates the contribution of IM products at a carrier frequency of ω_{c_1} and, (7d) and (7e) indicate the contribution of outer and inner CM products, respectively, at a carrier frequency of ω_{c_1}. Fig. 2 illustrates the location of IM as well as the inner and outer CM products of $y_{\omega_L}(t)$ expressed in (7).

Notice in Table I that when ω_L and ω_U are swept at the same rate, the frequency domain Volterra kernels are excited along diagonals in the frequency space, as seen in the argument of the frequency domain Volterra kernels in Table I. This is also the case for conventional two-tone tests [8]. Therefore, our results can be interpreted in ways similar to those of the conventional test.

In comparison with a conventional single-band transmitter, exciting a dual-band transmitter with a two two-tone signal results in additional terms, specifically, the outer CM products of $(\omega_L + 2\omega_U)$, $-(\omega_L + 2\omega_U)$ and inner CM products of $(\omega_L - 2\omega_U)$, $-(\omega_L - 2\omega_U)$ along with IM products of $(3\omega_L)$ and $-(3\omega_L)$ at the carrier frequency of ω_{c_1}. Therefore, in order to characterize the memory effects in a multi-band nonlinear transmitter, the analysis of both IM and CM products is required.

B. Analysis of IM and CM Products

In order to analyze the memory effects in a dual-band transmitter, an approach similar to a conventional two-tone test is suggested, i.e. each band is excited with a two-tone signal, which is symmetrical to their respective carrier frequencies. Furthermore, each two-tone test signal is designed such that $\Delta\omega_L > \Delta\omega_U$, where $\Delta\omega_U = 2\pi(\Delta_f)$ and $\Delta\omega_L = 2\pi(\Delta_f + \delta_f)$ with δ_f being a constant tone difference, and Δ_f, a varying tone difference.

The difference in tone spacing between the upper and lower band two-tone signals is essential in order to differentiate between IM and CM products, and to avoid overlapping of IM and CM products; Fig. 2 illustrates the respective positions of IM and CM products relative to the lower carrier frequency (ω_{c_1}). The proposed method is also applicable for the characterization of MIMO transmitters. In MIMO transmitters the different channels may have the same carrier frequencies. A frequency sweep is performed between 100 kHz and 10 MHz with $\delta_f = 100$ kHz and Δ_f varying with a step size of 0.1 MHz. The input power level is swept between -16 dBm and 1 dBm in steps of 0.09 dB.

For the characterization of memory effects in a dual-band amplifier, only the third IM and CM products are evaluated against frequency and power sweep. The power and frequency

TABLE I
COEFFICIENT OF (7) IN THE FORM OF FREQUENCY DOMAIN VOLTERRA KERNEL [8]

Number	h_m	Frequency domain Volterra kernels	Frequency	
1	$h_1^{(+)}$	$\mathrm{H}_1(\omega_{c_1}+\omega_L)$	$\omega_{c_1}+\omega_L$	(7a)
2	$h_1^{(-)}$	$\mathrm{H}_1(\omega_{c_1}-\omega_L)$	$\omega_{c_1}-\omega_L$	(7a)
3	$h_{3_{IM}}^{(+)}$	$\mathrm{H}_3(\omega_{c_1}+\omega_L,\omega_{c_1}+\omega_L,-\omega_{c_1}-\omega_L)$	$\omega_{c_1}+\omega_L$	(7b)
4	$h_{3_{IM}}^{(-)}$	$\mathrm{H}_3(\omega_{c_1}+\omega_L,\omega_{c_1}-\omega_L,-\omega_{c_1}-\omega_L)$	$\omega_{c_1}-\omega_L$	(7b)
5	$h_{3_{IM}}^{(+)}$	$\mathrm{H}_3(\omega_{c_1}+\omega_L,\omega_{c_1}+\omega_L,-\omega_{c_1}+\omega_L)$	$\omega_{c_1}+3\omega_L$	(7c)
6	$h_{3_{IM}}^{(-)}$	$\mathrm{H}_3(\omega_{c_1}-\omega_L,\omega_{c_1}-\omega_L,-\omega_{c_1}-\omega_L)$	$\omega_{c_1}-3\omega_L$	(7c)
7	$h_{3_{CM_{out}}}^{(+)}$	$\mathrm{H}_3(\omega_{c_1}+\omega_L,\omega_{c_2}+\omega_U,-\omega_{c_2}+\omega_U)$	$\omega_{c_1}+\omega_L+2\omega_U$	(7d)
8	$h_{3_{CM_{out}}}^{(-)}$	$\mathrm{H}_3(\omega_{c_1}-\omega_L,\omega_{c_2}-\omega_U,+\omega_{c_2}-\omega_U)$	$\omega_{c_1}-\omega_L-2\omega_U$	(7d)
9	$h_{3_{CM_{in}}}^{(+)}$	$\mathrm{H}_3(\omega_{c_1}-\omega_L,\omega_{c_2}+\omega_U,+\omega_{c_2}+\omega_U)$	$\omega_{c_1}-\omega_L+2\omega_U$	(7e)
10	$h_{3_{CM_{in}}}^{(-)}$	$\mathrm{H}_3(\omega_{c_1}+\omega_L,\omega_{c_2}-\omega_U,-\omega_{c_2}-\omega_U)$	$\omega_{c_1}+\omega_L-2\omega_U$	(7e)

sweep is performed simultaneously on both bands. For the evaluation of asymmetry between respective IM and CM products, 3-D energy surfaces can be used [22]. In 3-D energy surfaces, a smooth surface indicates a strong coherent contribution whereas a noise-like surface indicates weak or no contribution.

C. Identification of IM and CM products

In order to estimate the amplitudes and phases of IM and CM products, let $\tilde{y}_{\omega_L}(n)$ and $\tilde{y}_{\omega_U}(n)$ be the complex output signals of lower and upper bands of concurrent dual-band PA, the output signals can be modeled as

$$\begin{bmatrix} \mathbf{y}_{\omega_L} \\ \mathbf{y}_{\omega_U} \end{bmatrix} = \begin{bmatrix} \mathbf{H}_{\omega_L} & 0 \\ 0 & \mathbf{H}_{\omega_U} \end{bmatrix} \begin{bmatrix} \theta_{\omega_L} \\ \theta_{\omega_U} \end{bmatrix} + \begin{bmatrix} \mathbf{v}_1 \\ \mathbf{v}_2 \end{bmatrix}, \quad (8)$$

where $\mathbf{v}_1$, $\mathbf{v}_2$ are the measurement noise, $\mathbf{y}_{\omega_L}$ and $\mathbf{y}_{\omega_U}$ are the column vectors containing the measured and sampled output signals operating at lower and upper carrier frequencies, respectively,

$$\mathbf{y}_i = \begin{bmatrix} \mathbf{y}_i(0) \\ \mathbf{y}_i(Ts) \\ \vdots \\ \mathbf{y}_i((N-1)Ts) \end{bmatrix}, \quad i = [\omega_L\ \omega_U], \quad (9)$$

where Ts is the sampling time, and N is the number of samples. θ_{ω_L} and θ_{ω_U} are complex-valued column vectors containing the unknown amplitudes of IM and CM products in the lower and upper bands, respectively. For the lower band, θ_{ω_L} becomes

$$\theta_{\omega_L} = \begin{bmatrix} \theta_{-C_{out}}\ \theta_{-C_{in}}\ \theta_{-IM}\ \theta_{-\omega_L}\ \theta_{\omega_L}\ \theta_{IM}\ \theta_{C_{in}}\ \theta_{C_{out}} \end{bmatrix}^T. \quad (10)$$

The corresponding matrix $\mathbf{H}_{\omega_L}$ can be written as

$$\begin{bmatrix} 1 & 1 & \dots & 1 \\ e^{-jC_{out}T} & e^{-jC_{in}T} & \dots & e^{jC_{out}T} \\ \vdots & \vdots & \ddots & \vdots \\ e^{-jC_{out}(N-1)T} & e^{-jC_{in}(N-1)T} & \dots & e^{jC_{out}(N-1)T} \end{bmatrix},$$

where $C_{out} = (\omega_L + 2\omega_U)$ and $C_{in} = -(\omega_L - \omega_U)$ are the frequencies of outer and inner CM products, respectively, at ω_{c_1} and the frequencies of IM and CM products are known priori. The linear least square estimation (LSE) method [23] can be used to estimate the parameters θ_{ω_L} and θ_{ω_U}, respectively, as

$$J(\theta_i) = \underset{\theta_i}{arg\,min} \|y_i - \mathbf{H}_i\theta_i\|, \quad (11)$$

where J is the cost function. The LSE in (11) can be written in matrix form as

$$\hat{\theta}_i = (\mathbf{H}_i^*\mathbf{H}_i)^{-1}\mathbf{H}_i^*\mathbf{y}_i\,, \quad (12)$$

where '$*$' is the complex conjugate transpose. This method can be used to extract the amplitude and phase information of IM and CM products in time domain using digital baseband signal processing. This method has previously been used in [2] and [8] for the SISO PAs. Note that the above method can be extended for the evaluation of higher order IM and CM products. As seen in (8), the lower and upper band output signals are decoupled; a nonlinear dynamic MIMO system can be described as M MISO systems [24]. Thus, for a concurrent dual-band system it is not necessary to capture the upper and lower band signals simultaneously, thereby reducing the wideband analog-to-digital converter (ADC) requirement. In [17], the upper and lower band signals of a concurrent dual-band PA is captured in two steps i.e., the analog-to-digital conversion is done by tuning the center frequency of the vector spectrum analyzer to digitize the lower and upper-band signals separately.

III. Experimental Setup

The experimental setup is shown in Fig. 1. The test signals were generated using Matlab and consist of two two-tone signals, one for each concurrent band. The complex baseband signals generated were uploaded to the baseband generators of two R&S SMBV100a vector signal generators (VSG), i.e., each generated a two-tone signal, which was then up-converted to RF. Note that the two two-tone signals can also be generated using a single VSG, but due to the hardware constraints, it was not possible to generate a wideband signal, as the VSG was limited to a maximum signal bandwidth of 120 MHz. As mentioned earlier, in concurrent dual-band transmitters, the difference between operating carrier frequencies is hundreds of MHz to GHz [15]–[17], therefore it is convenient to use multiple VSGs.

The generated RF signals, operating at two different carrier frequencies, were combined using a HP 87302C power combiner. The combined RF signal was fed to the device under test (DUT). The output RF signal was down-converted to an IF signal using a wideband down-converter. Since the output signal has two operational carrier frequencies, the local oscillator (LO) frequency of the down-converter can be tuned for down-converting the upper and/or lower-band, which reduces the hardware requirement. The IF signal is fed to an SP-devices-ADQ-214 ADC to digitize the signal. The performance of the measurement setup was limited to a -71-dB adjacent channel power ratio.

Two different amplifiers were used as DUTs: a wide-band PA (model ZVE8G+ amplifier of Mini-Circuits Inc., Brooklyn, NY) and a Freescale Doherty PA (transistor model MRF8S21120HS-Doherty of Freescale Inc., Austin, TC). The ZVE8G+ amplifier has a nominal small signal gain of 30 dB and an output 1 dB compression point of 30 dBm, whereas, the Freescale Doherty PA has a gain of 15 dB and an output 1 dB compression point of 46 dBm. The first amplifier was used to illustrate the method, whereas the Doherty amplifier was used for the comparison of CM products and to analyze how the physics of the PA changes the asymmetric energy surfaces. Carrier frequencies for the lower and upper band were 2 GHz and 2.3 GHz, respectively, for both tested amplifiers.

The test signal's amplitude distribution can be important when measuring nonlinear effects, therefore, the peak-to-average power ratio (PAPR) of the combined signal was measured at the PA's input and was found to be 5.98 ± 0.02 dB for all test signals. Moreover, the two-tone signals consist of 20000 samples each at a sampling rate of 80 MHz. To improve the performance of the measurement system, 200 coherent averages were performed [25].

A. Error Analysis and System Calibration

The distortion of the input signals of DUT can influence the measurement and introduce errors. These distortions can be either from the noisy RF sources or from the linear/nonlinear distortions of the input signals. To compensate for these effects, both SMBV100a VSGs were fed with two external LO signals for up-converting the two baseband signals to their respective RF signals, instead of using the internal LO of the

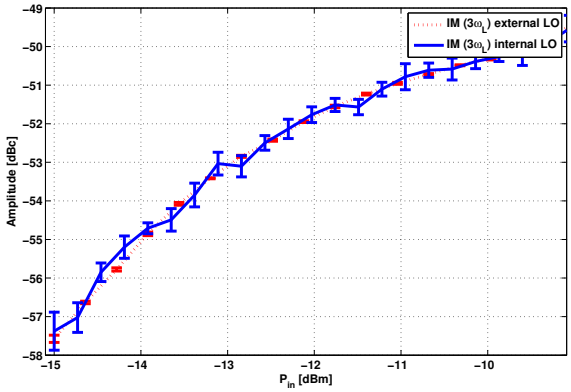

Fig. 3. Measured relative amplitude of upper IM product with internal and external (dotted) LO sources over the input power range of -15 to -9 dBm at the carrier frequency of 2 GHz. The error bars indicates the amplitude standard deviation of 10 repeated measurements. The DUT was ZVE8G amplifier.

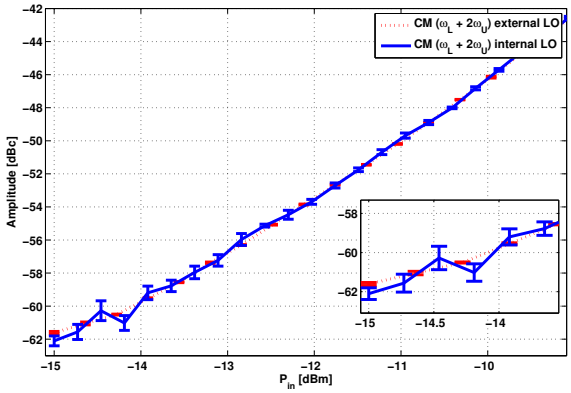

Fig. 4. Measured relative amplitude of outer CM product with internal and external (dotted) LO sources over the input power range of -15 to -9 dBm at the carrier frequency of 2 GHz. The error bars indicates the amplitude standard deviation of 10 repeated measurements. The DUT was ZVE8G amplifier.

VSGs. These LO signals were generated by the Holzworth HS9003A RF synthesizer.

Figs. 3 and 4 show the measured amplitude of the upper IM ($3\omega_L$) and outer CM ($\omega_L + 2\omega_U$) product relative to the carrier frequency of 2 GHz, when the internal and external LO sources were used to up-convert the baseband signals of the VSGs to their respective carrier frequencies. The error bars indicate the IM/CM amplitude standard deviations of 10 repeated measurements. The effect of noise in the respective RF sources can be observed in Figs. 3 and 4, where the standard deviation in measured IM products is between [0.04 and 0.58] and [0.009 and 0.16] for internal and external LO sources, respectively. For outer CM product, standard deviation lies between [0.01 and 0.63] and [0.008 and 0.13] for internal and external LO sources, respectively.

Figs. 5 and 6 show the phase behavior versus the input power range for upper IM and outer CM products. One can clearly see that the measured phase is sensitive to noise in the RF source when the internal LOs were used. For the upper IM product, the maximum and minimum phase standard deviation

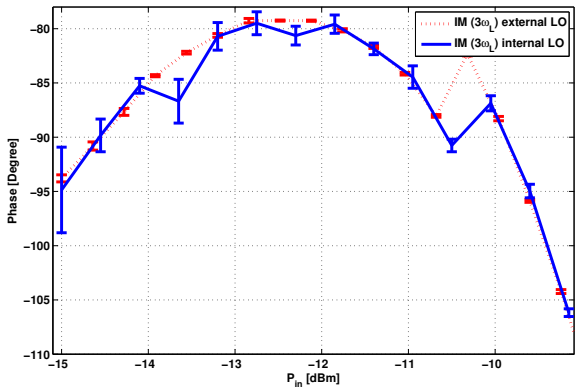

Fig. 5. Measured relative phase of upper IM product with internal and external (dotted) LO sources over the input power range of -15 to -9 dBm at the carrier frequency of 2 GHz. The error bars indicates the phase standard deviation of 10 repeated measurements. The DUT was ZVE8G amplifier.

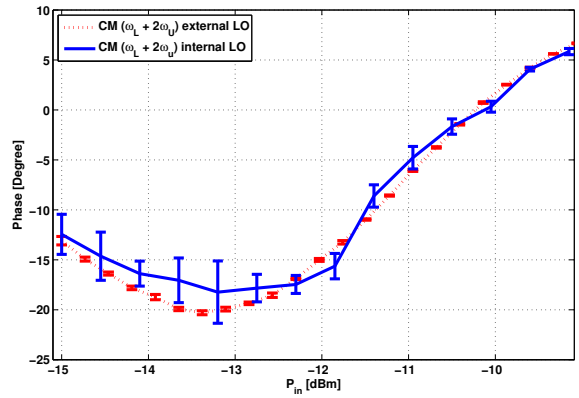

Fig. 6. Measured relative phase of upper CM product with internal and external (dotted) LO sources over the input power range of -15 to -9 dBm at the carrier frequency of 2 GHz. The error bars indicates the phase standard deviation of 10 repeated measurements. The DUT was ZVE8G amplifier.

is between [0.018 and 0.5] degrees when the external LOs were used, whereas, in the case of the internal LOs, the phase standard deviation lies in the range of [0.28 and 3.9] degrees. Similarly, the maximum and minimum standard deviation for CM product is between [0.015 and 0.59] degrees when the external LOs were used and with internal LOs, the standard deviation is between [0.18 and 3.62] degrees. Furthermore, the above results indicate that compared with the external LOs, the internal LOs are sensitive to noise when the input power level is low.

Figs. 3-6 are important results, as they illustrate the accuracy and repeatability of the measurement system. Additionally, these results are also important when a DPD algorithm is applied for the linearization of concurrent or MIMO transmitters. In DPD, the pre-distorted signals have the same amplitude but opposite phase to compensate for the distortions produced by the nonlinear transmitter. Thus, if the phase and amplitude variations over repeated measurements are high, then the linearization performance will be degraded. These effects are reported in [19], where linearization was performed on a 2×2 MIMO transmitter.

The linear/nonlinear distortions of the input signals could be compensated by measuring the input to the DUT and subtracting the distortion products from the output signal. The linear distortion in the input signals is due to the frequency dependency and the nonlinear distortions are due to the internal amplifier of the VSG [26]. Since these distortion products are significantly smaller than the fundamentals and IM/CM products, they do not generate significant distortion and were not considered in this study. In order to compensate for these effects, an approach similar to [2] could be applied. Moreover, the systematic errors caused by the cables, connectors and the room temperature were not analyzed in this study. The spurious free dynamic range of the measurement setup was -71 dB.

B. Metrics for Evaluation

Asymmetric Energy Surfaces and 2-D plot: For the evaluation of IM and CM products, excitation signals were swept both in frequency and power. The sweeping was performed such that for a certain value of Δ_f and $\Delta_f + \delta_f$, the input power of the two two-tone signals was swept from a minimum to a maximum power level. When this sweep was completed, the next value for Δ_f and $\Delta_f + \delta_f$ was chosen and the amplitude sweep was repeated again. This creates a 3-D matrix (i.e., dimension for frequency, power, and measured amplitude).

Based upon these measurements, asymmetric 3-D energy surfaces were plotted by subtracting the upper IM and CM products from their corresponding lower IM and CM products, respectively. As such the amount of asymmetry between the IM and CM products, respectively can be determined. The asymmetry between IM products can be defined as

$$\text{IM}_{asymmetry} = 20 \times \log_{10}(\frac{IM_U}{IM_L}) = IM_{U_{dB}} - IM_{L_{dB}}, \tag{13}$$

where IM_U and IM_L are upper and lower IM products determined by solving (8).

Apart from 3-D energy surfaces, measurement results are also presented in the classical 2-D plots for both frequency and input power sweep. For the power sweep, the measured IM and CM amplitudes were also evaluated against a 3:1 slope. The 3:1 slope illustrates that the amplitudes of the IM/CM tones are proportional to the third power of the input amplitude [27].

IV. RESULTS

The two two-tone signals operating at the carrier frequencies of 2 and 2.3 GHz, respectively, were swept in both power and frequency. Measurements were done on a wideband Mini-circuit ZVE8G PA. Below, we present only the magnitude of the IM and CM products. The magnitude is more often analyzed in the conventional two-tone tests; also, due to dispersion relations, structures in the magnitude's frequency dependence have corresponding structures in the phase [8], [28], which was also observed in this study. The result of the power sweep is shown in Fig. 7 for IM products for

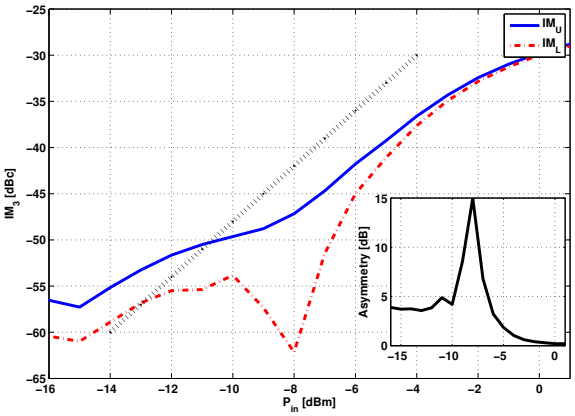

Fig. 7. Measured amplitude of upper (blue) and lower (red) IM product relative to the carrier frequency of 2 GHz with tone spacing of $\Delta_f+\delta_f = 500$ kHz and $\Delta_f = 400$ kHz, where fundamental tones were at a carrier frequency of 2 GHz and 2.3 GHz. Black dotted line indicates the 3:1 amplitude slope. The inset shows the amount of asymmetry between IM products. The DUT was a ZVE8G amplifier. For Pin = 0 dBm, DUT goes into 1-dB compression point

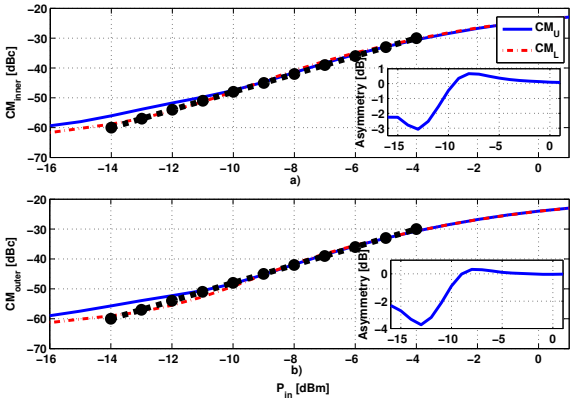

Fig. 8. Measured amplitude of inner (a) and outer (b) CM products relative to the carrier frequency of 2 GHz with tone separation of $\Delta_f+\delta_f = 500$ kHz and $\Delta_f = 400$ kHz, where fundamental tones were at a carrier frequency of 2 GHz and 2.3 GHz. A 3:1 dB slope is indicated by a black dotted line. The DUT was a ZVE8G amplifier. For Pin = 0 dBm, DUT goes into 1-dB compression point

a tone spacing of 500 kHz operating at a carrier frequency of 2 GHz, whereas the upper two-tone signal had a tone spacing of 400 kHz. At 0 dBm input power, DUT goes into 1-dB compression point. The dotted line indicates the 3:1 slope. The results indicate that the amplitudes of upper and lower IM tones are not proportional to the third power of the fundamental tones. Such behavior illustrates that the IM products are not purely due to third degree nonlinearities [27]. Furthermore, the asymmetry between upper and lower IM products is significant, indicating the presence of memory effects [2]. The inset shows the asymmetry between the upper and lower IM products which reaches a maximum at an input power of -8 dBm. The asymmetry reduces to 0 dB at high power levels (the PA goes into compression), indicating reduced asymmetry and hence reduced memory effects that contribute to the asymmetry [28]. The notch in the lower IM product is due to the opposite phases of third and fifth degree coefficients [27].

Fig. 8 (a and b) shows the result of the amplitude sweep for inner and outer CM products, respectively. The CM products were measured at the carrier frequency of 2 GHz, whereas the two-tone signal was at a carrier frequency of 2.3 GHz and had a tone spacing of 400 kHz. Fig. 8 illustrates that the amplitudes of lower inner and lower outer CM products approximately increase to the third power of the input signal as indicated by the 3:1 slope. The amplitudes of upper inner and upper outer CM products deviate slightly from the 3:1 slope.

The inset in Fig. 8 shows that inner and outer CM products have approximately the same asymmetric behavior. Compared with the IM products, CM products have reduced asymmetry, indicating that the memory effects that cause asymmetry are lower. Furthermore, Figs. 7 and 8 indicate that as the input power increases, the asymmetry reduces in both IM and CM products. The reduction in the asymmetry is because the PA enters into compression.

As mentioned earlier, memory effects can be quantified as a measure of frequency dependency versus tone spacing. Moreover, memory effects can be categorized into electrical memory effects (short term memory effects) and electrothermal memory effects (long term memory effects) [29]. Electrical memory effects can be considered as the main source of memory effects in PAs when driven by wideband signals, e.g., WCDMA signals. However, in case of narrow bandwidth signals, e.g., signals with the bandwidth of smaller than a few hundred kHz (GSM), electrothermal memory effects dominate [29]. The amplifiers used in this study are driven by signals with frequency separation of 400 kHz upto 20 MHz, therefore, electrical memory effects are considered as the main source of memory effects.

Fig. 9 and Fig. 10 (a and b) show the result of memory effects quantified as measure of frequency dependency versus tone spacing for IM and CM products, respectively, at an input power level of -6 dBm. A considerable asymmetry between the upper and lower IM products is clearly observed at lower tone spacing (cf Fig. 9), for tone spacing < 1 MHz, indicating that the PA exhibits considerable memory effects in this region. The comparison between Fig. 10 a and b indicates that the inner CM products have slightly higher asymmetry than the outer CM products. Two things can clearly be observed from Figs. 9 and 10. First, the IM products exhibit notable memory effects compared to the CM products as the amplitude of IM products degrades more with an increase in tone spacing as compared to CM products. Second, the amplitude levels of IM and CM products are quite different at the same input power level. Eqn. (7) shows that the amplitude of the IM product is less than that of the CM product by a factor of 2.

The frequency dependence of the IM products in a conventional two-tone test can be explained by the feed back structure of a PA [27]. The RF signal is down-converted to baseband and then up-converted to RF in the power amplifier. Thus, memory effects at baseband frequencies are excited [8]. The same memory effects will also be excited in the dual two-tone

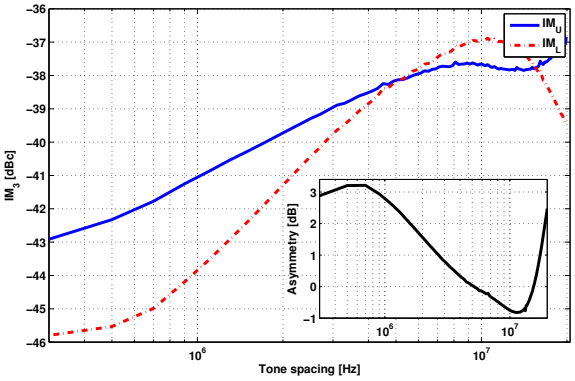

Fig. 9. Measured amplitude of IM products relative to a carrier frequency of 2 GHz at an input power level of -6 dBm as a function of tone spacing. The inset shows the amount of asymmetry between upper and lower IM products. The DUT was ZVE8G amplifier.

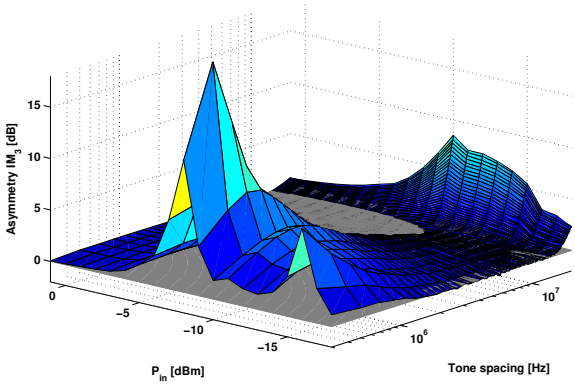

Fig. 11. Asymmetric energy surface between lower and upper IM products. Symmetric surface is shown by the gray plane. The DUT was ZVE8G amplifier.

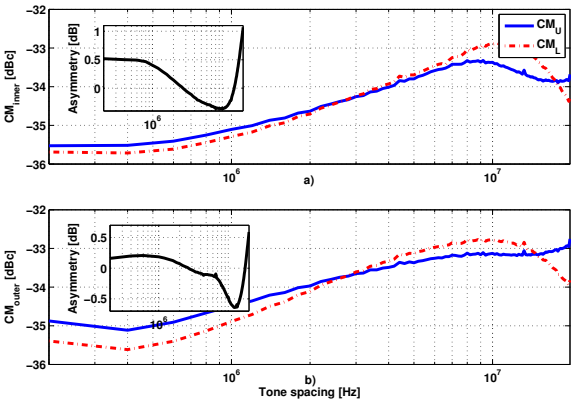

Fig. 10. Measured amplitude of CM products relative to a carrier frequency of 2 GHz at an input power level of -6 dBm as a function of tone spacing. The inset shows the amount of asymmetry between upper and lower CM products. The DUT was ZVE8G amplifier.

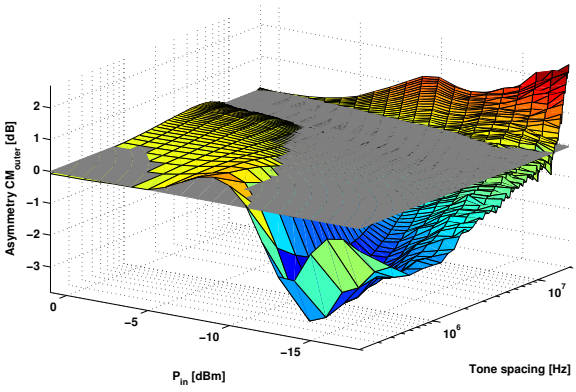

Fig. 12. Asymmetric energy surface between outer CM products. The gray surface indicates symmetric CM products. The DUT was ZVE8G amplifier.

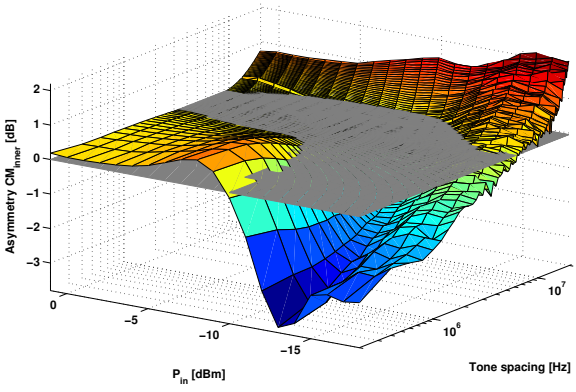

Fig. 13. Asymmetric energy surface between inner CM products. The gray surface indicates symmetric CM products. The DUT was ZVE8G amplifier.

test and seen in both IM and CM products. In addition, the CM products will be affected by a down-conversion to the frequency $\omega_{c_2} - \omega_{c_1}$ and then up converted to ω_{c_1} and ω_{c_2}, respectively. In this case, the memory effects at $\omega_{c_2} - \omega_{c_1}$ are smaller than those at baseband frequencies. Hence, the CM and IM asymmetry have some quantitative similarities; it decreases to a minimum at $\sim$ 10 MHz. The asymmetry magnitude is, however, smaller for the CM than the IM products.

The asymmetric energy surface for the IM product is shown in Fig. 11, where the gray plane indicates the symmetric region, i.e., where the upper and lower IM products have the same amplitude. Fig. 11 shows that for a tone spacing of $<$1 MHz and for an input power level of $\leq$ -4 dBm, the asymmetry between the upper and lower IM products is significant, indicating that the PA has more memory effects under these conditions. The maximum asymmetry observed is 15 dB at an input power of -8 dBm (cf Fig. 7). For an input power $>$ -4 dBm and over the complete frequency range, the asymmetry between upper and lower IM products is less than 1 dB. Thus, for high input power levels, the measured PA has low asymmetry as it goes into compression. It is important to note that asymmetry implies memory effects, but no asymmetry alone does not imply no memory effects. Furthermore, for tone spacing $\geq$ 15 MHz and input power levels of -14 to -5 dBm, the asymmetry increases to a maximum level of 5 dB. Figs. 12 and 13 show the asymmetric behavior of outer

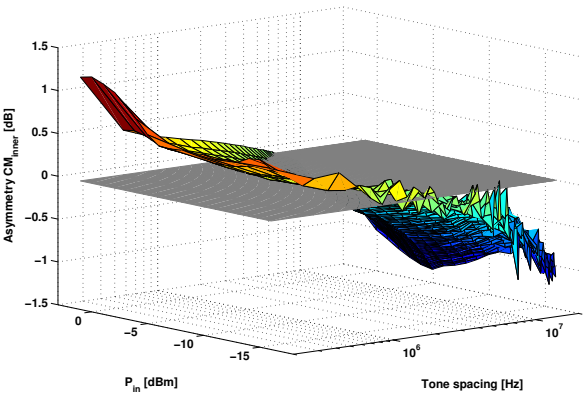

Fig. 14. Asymmetric energy surface between inner CM products when the Doherty amplifier was used. The gray surface indicates symmetric CM products.

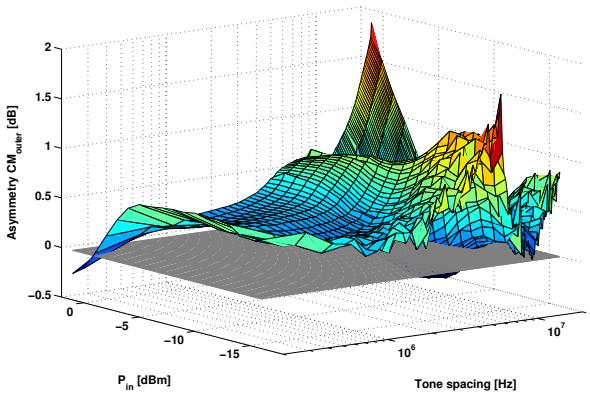

Fig. 15. Asymmetric energy surface between outer CM products when the Doherty amplifier was used. The gray surface indicates symmetric CM products.

and inner CM products. The comparison between the energy surfaces of two CM products indicates approximately the same asymmetric behavior. For an input power of $\geq$ -5 dBm and tone spacing of 200 kHz to 3 MHz, the asymmetry between the upper and lower CM products is less than 1 dB for both outer and inner CM products. For higher frequency ranges, the asymmetry of inner CM products is slightly larger than that for the outer CM products. For the tone spacing of 200 kHz to 500 kHz, and between -18 to -11 dBm input power levels, the inner CM product has a slightly higher asymmetry than the outer CM product. The maximum measured asymmetric level was approximately 3.5 dB at a tone spacing of 200 kHz. Compared with outer CM products, at the input power level $>$ -5 dBm and at high tone spacing, the asymmetry between inner CM products is high.

A noticeable difference in the overall asymmetric behavior of IM and CM products can be observed in Figs 11, 12 and 13, where IM products tend to have larger memory effects that contribute to asymmetry compared to the CM products. This information can be utilized for the optimization of behavioral models and digital pre-distorters e.g., 2-D DPD model published in [30] where the model use same memory depth for IM and CM products. As mentioned earlier, the asymmetric behavior of IM and CM products reduces at an input power level $>$ -5 dBm as the PA goes into compression.

Figs. 14 and 15 show the asymmetric energy surfaces of the CM products when a Doherty amplifier was used. A considerable difference between the asymmetric behavior of inner and outer CM products can be observed in Figs. 14 and 15, indicating that the memory effects are different for inner and outer CM products, compared to the energy surfaces of inner and outer CM products when the Mini-Circuit ZVE8G amplifier was used. These results indicate that the asymmetric behavior varies with different DUTs. The change in asymmetric behavior is due to different physical structures of the DUTs.

The asymmetric energy surfaces can be used to identify the power and frequency regions of the IM and CM products where the memory effects that contribute to the asymmetry are large. Furthermore, the analysis can also be used to evaluate the similarity between the asymmetry energy surfaces for the IM and CM products. As seen in Figs. 12 and 13, the asymmetric energy surfaces of inner and outer CM products are approximately the same for the ZVE8G wide-band amplifier, which indicates that the memory effects that contribute to the asymmetry are approximately the same for outer and inner CM products. Figs. 14 and 15, show a considerable difference between the asymmetric energy surfaces of the outer and inner CM products of the Doherty amplifier, which indicates that the memory effects that contribute to asymmetry are different for outer and inner CM products.

V. Conclusion

This paper proposed a method for the characterization of memory effects in concurrent dual-band amplifiers. Measurement results for the ZVE8G amplifier indicated that the third-order IM products have dominant memory effects compared to CM products while the inner and outer CM products have approximately the same memory effects, as illustrated by the energy surfaces. Contrary to the ZVE8G amplifier, measurements of the Doherty amplifier showed that the inner and outer CM products have different asymmetry surfaces, indicating different memory effects that contribute to asymmetry of the inner and outer CM products.

The proposed method can be used prior to the implementation of DPD algorithms for the linearization of nonlinear multi-band transmitters. The information of memory effects extracted from third and higher order IM and CM products can be utilized to optimize the parametric memory polynomial models in terms of nonlinear order and memory depth for the DPD applications.

In Section III-A, the effects of a noisy RF source have been studied. For the linearization of a concurrent dual-band transmitter, it is important to have a phase stable RF source, as linearization algorithms use signals with the same amplitudes, but use the opposite phases of distorting signals. Therefore, due to the phase and amplitude variations, the linearization performance will be degraded.

APPENDIX
MATHEMATICAL STEPS FOR (4)

By using trigonometric property on a, b, c and d terms in (4) results in following frequency components,

$$\underbrace{\cos^3(\omega_L t)\cos^3(\omega_{c_1} t)}_{\text{a}} = \tag{A.14a}$$

$$\frac{1}{16}\{(3\cos(\omega_L t)+\cos(3\omega_L t))(3\cos(\omega_{c1} t)+\cos(3\omega_{c1} t))\} = \tag{A.14b}$$

$$\frac{1}{16}\left[9\cos(\omega_L t)cos(\omega_{c1} t)+3\cos(3\omega_{c1} t)\cos(\omega_L t)+\right. \tag{A.14c}$$

$$3\cos(\omega_{c1} t)\cos(3\omega_L t)+\cos(3\omega_{c1} t)\cos(3\omega_L t)] = \tag{A.14d}$$

$$\frac{1}{16}\left[\underbrace{\{9\cos(\omega_L t)+3\cos(3\omega_L t)\}\cos(\omega_{c1} t)}_{\text{terms at } \omega_{c1}}+\right. \tag{A.14e}$$

$$\left.\underbrace{\{3\cos(3\omega_L t)+\cos(3\omega_L t)\}\cos(\omega_{3c1} t)}_{\text{terms at } 3\omega_{c1}}\right]. \tag{A.14f}$$

Eqn. (A.14e) shows the frequency components closed to the carrier frequency ω_{c1}, the frequency components given in (A.14f) can be filtered out. Applying trigonometric property on b in (4) results in following frequency components,

$$\underbrace{\cos^3(\omega_U t)\cos^3(\omega_{c_2} t)}_{\text{b}} = \tag{A.15a}$$

$$\frac{1}{16}\{(3\cos(\omega_U t)+\cos(3\omega_U t))(3\cos(\omega_{c2} t)+\cos(3\omega_{c2} t))\} = \tag{A.15b}$$

$$\frac{1}{16}\left[9\cos(\omega_U t)cos(\omega_{c2} t)+3\cos(3\omega_{c2} t)\cos(\omega_U t)+\right. \tag{A.15c}$$

$$3\cos(\omega_{c2} t)\cos(3\omega_U t)+\cos(3\omega_{c2} t)\cos(3\omega_U t)] = \tag{A.15d}$$

$$\frac{1}{16}\left[\underbrace{\{9\cos(\omega_U t)+3\cos(3\omega_U t)\}\cos(\omega_{c2} t)}_{\text{terms at } \omega_{c2}}+\right. \tag{A.15e}$$

$$\left.\underbrace{\{3\cos(3\omega_U t)+\cos(3\omega_U t)\}\cos(3\omega_{c2} t)}_{\text{terms at } 3\omega_{c2}}.\right] \tag{A.15f}$$

Eqn. (A.15e) shows the frequency components at the carrier frequency ω_{c2}, the frequency components given (A.15f) can be filtered out. Applying trigonometric property on c in (4) results in following frequency components,

$$\underbrace{3\cos^2(\omega_L t)\cos^2(\omega_{c_1} t)\cos(\omega_U t)\cos(\omega_{c_2} t)}_{\text{c}} = \tag{A.16a}$$

$$\frac{3}{4}\left[\underbrace{\cos(2\omega_L t)\cos(2\omega_{c1} t)\cos(\omega_{c2} t)\cos(\omega_U t)}_{\text{terms not at fundamental frequencies}}+\right. \tag{A.16b}$$

$$\underbrace{\cos(2\omega_{c1} t)\cos(\omega_{c2} t)\cos(\omega_U t)}_{\text{terms at } 2\omega_{c1}\pm\omega_{c2}}+ \tag{A.16c}$$

$$\left.\underbrace{\{\cos(\omega_U)+\cos(2\omega_L t)\cos(\omega_{c2} t)\}\cos(\omega_U t)}_{\text{terms at } \omega_{c2}}\right]. \tag{A.16d}$$

Eqn. (A.16d) shows the frequency components due to cross-modulation between the two two-tones signals at the carrier frequency ω_{c2}. Frequency components given by (A.16b) and (A.16c) can be filtered out. Applying trigonometric property on d in (4) results in following frequency components,

$$\underbrace{3\cos^2(\omega_U t)\cos^2(\omega_{c_2} t)\cos(\omega_L t)\cos(\omega_{c_1} t)}_{\text{d}} = \tag{A.17a}$$

$$\frac{3}{4}\left[\underbrace{\cos(2\omega_U t)\cos(2\omega_{c2} t)\cos(\omega_{c1} t)\cos(\omega_L t)}_{\text{terms not at fundamental frequencies}}+\right. \tag{A.17b}$$

$$\underbrace{\cos(2\omega_{c2} t)\cos(\omega_{c1} t)\cos(\omega_L t)}_{\text{terms at } 2\omega_{c2}\pm\omega_{c1}}+ \tag{A.17c}$$

$$\left.\underbrace{\{\cos(\omega_L)+\cos(2\omega_U t)\cos(\omega_{c1} t)\}\cos(\omega_L t)}_{\text{terms at } \omega_{c1}}\right]. \tag{A.17d}$$

Similarly, (A.17d) shows the frequency components due to cross-modulation between the two two-tones signals at the carrier frequency ω_{c1}. Frequency components given by (A.17b) and (A.17c) can be filtered out.

REFERENCES

[1] D. M. Pozar, *Microwave Engineering, 4th ed.* Hoboken, NJ, USA: John Wiley, 2011.

[2] D. Wisell, B. Rudlund, and D. Rönnow, "Characterization of memory effects in power amplifiers using digital two-tone measurements," *IEEE Trans. Instru. and Meas.*, vol. 56, no. 6, pp. 2757–2766, Dec 2007.

[3] J. Vuolevi, T. Rahkonen, and J. Manninen, "Measurement technique for characterizing memory effects in RF power amplifiers," *IEEE Trans. Microw. Theory Techn.*, vol. 49, no. 8, pp. 1383–1389, Aug 2001.

[4] H. Ku, M. Mckinley, and J. Kenney, "Quantifying memory effects in RF power amplifiers," *IEEE Trans. Microw. Theory Techn.*, vol. 50, no. 12, pp. 2843–2849, Dec 2002.

[5] K. Remley, D. Williams, D. M. M. P. Schreurs, and J. Wood, "Simplifying and interpreting two-tone measurements," *IEEE Trans. Microw. Theory Techn.*, vol. 52, no. 11, pp. 2576–2584, Nov 2004.

[6] J. Martins, P. Cabral, N. Carvalho, and J. Pedro, "A metric for the quantification of memory effects in power amplifiers," *IEEE Trans. Microw. Theory Techn.*, vol. 54, no. 12, pp. 4432–4439, Dec 2006.

[7] J. Pedro and J. Martins, "Amplitude and phase characterization of nonlinear mixing products," *IEEE Trans. Microw. Theory Techn.*, vol. 54, no. 8, pp. 3237–3245, Aug 2006.

[8] D. Rönnow, D. Wisell, and M. Isaksson, "Three-Tone characterization of nonlinear memory effects in radio-frequency power amplifiers," *IEEE Trans. Instru. and Meas.*, vol. 56, no. 6, pp. 2646–2657, Dec 2007.

[9] R. Westcott, "Investigation of multiple FM/FDM carriers through a satellite TWT operating near to saturation," *Proc. IEEE*, vol. 114, no. 6, pp. 726–740, June 1967.

[10] C. Rauscher and R. Tucker, "Method for measuring 3rd-order intermodulation distortion in GaAs FETs," *Electron. Lett.*, vol. 13, no. 23, pp. 701–702, November 1977.

[11] N. Suematsu, Y. Iyama, and O. Ishida, "Transfer characteristic of IM3 relative phase for a GaAs FET amplifier," *IEEE Trans. Microw. Theory Techn.*, vol. 45, no. 12, pp. 2509–2514, Dec 1997.

[12] Y. Yang, J. Yi, J. Nam, B. Kim, and M. Park, "Measurement of two-tone transfer characteristics of high-power amplifiers," *IEEE Trans. Microw. Theory Techn.*, vol. 49, no. 3, pp. 568–571, Mar 2001.

[13] C. Crespo-Cadenas, J. Reina-Tosina, and M. J. Madero-Ayora, "Phase characterization of two-tone intermodulation distortion," in *IEEE MTT-S Int. Microw. Symp. Dig.*, June 2005, pp. 1505–1508.

[14] Y. Shen, "Computation-based phase measurement of RF power-amplifier intermodulation products," *IEEE Trans. Instru. and Meas.*, vol. 60, no. 8, pp. 2934–2941, Aug 2011.

[15] W. Chen, S. Bassam, X. Li, Y. Liu, K. Rawat, M. Helaoui, F. Ghannouchi, and Z. Feng, "Design and linearization of concurrent dual-band Doherty power amplifier with frequency-dependent power ranges," *IEEE Trans. Microw. Theory Techn.*, vol. 59, no. 10, pp. 2537–2546, Oct 2011.

[16] W. Chen, S. Bassam, M. Helaoui, F. Ghannouchi, and Z. Feng, "Characterization of memory effects in concurrent dual-band PAs," in *Asia-Pacific Microw. Conf.*, Dec 2011, pp. 1646–1649.

[17] Y.-J. Liu, W. Chen, J. Zhou, B.-H. Zhou, and F. Ghannouchi, "Digital predistortion for concurrent dual-band transmitters using 2-d modified memory polynomials," *IEEE Trans. Microw. Theory Techn.*, vol. 61, no. 1, pp. 281–290, Jan 2013.

[18] S. Bassam, M. Helaoui, and F. Ghannouchi, "Crossover digital predistorter for the compensation of crosstalk and nonlinearity in MIMO transmitters," *IEEE Trans. Microw. Theory Techn.*, vol. 57, no. 5, pp. 1119–1128, May 2009.

[19] S. Amin, P. N. Landin, P. Händel, and D. Rönnow, "Behavioral modeling and linearization of crosstalk and memory effects in RF MIMO transmitters," *IEEE Trans. Microw. Theory Techn.*, vol. 62, no. 4, pp. 810–823, April 2014.

[20] Y. Palaskas, A. Ravi, S. Pellerano, B. Carlton, M. Elmala, R. Bishop, G. Banerjee, R. Nicholls, S. Ling, N. Dinur, S. Taylor, and K. Soumyanath, "A 5-GHz 108-Mb/s 2x2 MIMO Transceiver RFIC With Fully Integrated 20.5-dbm P_1dB power amplifiers in 90-nm CMOS," *IEEE J. Solid-State Circuits*, vol. 41, no. 12, pp. 2746–2756, 2006.

[21] A. Zhu and T. Brazil, "Behavioral modeling of RF power amplifiers based on pruned volterra series," *IEEE Microw. Compon. Lett.*, vol. 14, no. 12, pp. 563–565, Dec 2004.

[22] W. Van Moer and Y. Rolain, "A large-signal network analyzer: Why is it needed?" *IEEE Microw. Mag.*, vol. 7, no. 6, pp. 46–62, 2006.

[23] S. M. Kay, *Fundamentals of Statistical Signal Processing: Estimation theory, 4th ed.* Upper Saddle River, NJ, USA: Prentice-Hall PTR, 1998.

[24] A. K. Swain and S. A. Billings, "Generalized frequency response function matrix for mimo non-linear systems," *Int. J. Control*, vol. 74, no. 8, pp. 829–844, 2001.

[25] "IEEE standard for terminology and test methods for analog-to-digital converters," *IEEE Std 1241-2000*, pp. i–, 2001.

[26] J. Jin and J. Peng, "Dynamic pre-compensation of memory nonlinear distortion for high-speed signal generator based on volterra inverse," in *Int. Conf. Commun. Mobile Comput.*, vol. 3, April 2010, pp. 142–146.

[27] V. Joel and R. Timo, *Distortion in RF Power Amplifiers*. Boston London: Artech Hourse, 2003.

[28] J. Kenney and P. Fedorenko, "Identification of RF power amplifier memory effect origins using Third-Order Intermodulation Distortion Amplitude and Phase Asymmetry," in *IEEE Int. Microw. Symp. Dig.*, June 2006, pp. 1121–1124.

[29] S. Boumaiza and F. Ghannouchi, "Thermal memory effects modeling and compensation in RF power amplifiers and predistortion linearizers," *IEEE Trans. Microw. Theory Techn.*, vol. 51, no. 12, pp. 2427–2433, Dec 2003.

[30] S. Bassam, W. Chen, M. Helaoui, F. Ghannouchi, and Z. Feng, "Linearization of Concurrent Dual-Band Power Amplifier based on 2D-DPD Technique," *IEEE Microw. Compon. Lett*, vol. 21, no. 12, pp. 685–687, Dec 2011.

Shoaib Amin (S'12) received the B.Eng degree in Avionics Engineering from College of Aeronautical Engineering (CAE), National University of Sciences and Technology, Islamabad, Pakistan in 2008, the M.Sc. degree in Electronics and Telecommunication from the University of Gävle, Gävle, Sweden in 2011. In 2012, he joined University of Gävle and KTH Royal Institute of Technology where he is currently working towards the Ph.D degree. In 2015, he received the degree of Licentiate in Engineering from KTH Royal Institute of Technology, Stockholm, Sweden.

His current research interests include measurement and signal processing techniques for modeling multiple-input multiple-output (MIMO) and concurrent multi-band radio frequency power amplifiers.

Wendy Van Moer (S'97-M'01-SM'07) received the M.Eng. and Ph.D. degrees in Engineering from the Vrije Universiteit Brussel (VUB), Brussels, Belgium, in 1997 and 2001, respectively.

She is currently a Visiting Professor at the Department of Electronics, Mathematics and Natural Sciences, University of Gävle, Gävle, Sweden. Her main research interests are nonlinear measurement and modeling techniques for medical and high-frequency applications. She has published over 100 related conference/peer reviewed journal articles.

Dr. Van Moer was the recipient of the 2006 Outstanding Young Engineer Award from the IEEE Instrumentation and Measurement Society. Since 2007, she has been an Associate Editor for the IEEE Transactions on Instrumentation and Measurement. From 2010 till 2012, she was an Associate Editor for the IEEE Transactions on Microwave Theory and Techniques.

In 2012, she was elected as a member of the administrative committee of the IEEE Instrumentation and Measurement society for a 4-year term. Since 2014, she is the editor-in-chief of the IEEE Instrumentation and Measurement Magazine.

Peter Händel (S'88-M'94-SM'98) received the M.Sc. degree in engineering physics and the Ph.D. degree in automatic control from Uppsala University, Uppsala, Sweden, in 1987 and 1993, respectively.

In 1987 and 1988, he was with the Svedberg Laboratory, Uppsala University. From 1988 to 1993, he was with the Systems and Control Group, Uppsala University. In 1996, he was appointed as Docent at Uppsala University. From 1993 to 1997, he was with the Research and Development Division, Ericsson AB, Kista, Sweden. During 19961997, he was a visiting Scholar at the Signal Processing Laboratory, Tampere University of Technology, Tampere, Finland. In 1998, he was appointed as Docent at the Tampere University of Technology. Since 1997, he has been with the Department of Signal Processing, Royal Institute of Technology, Stockholm, Sweden, where he is currently a Professor of signal processing. He has authored approximately 95 journal articles and 150 conference papers and is the holder of 15 patents. He has conducted research on the design and analysis of digital filters and adaptive filters, measurement and estimation theory (particularly, temporal frequency estimation), system identification, speech processing, and measurement methods for characterization of analog-to-digital converters and power amplifiers.

Daniel Rönnow received the M.Sc. degree in engineering physics and Ph.D. degree in solid-state physics from Uppsala University, Uppsala, Sweden, in 1991 and 1996, respectively.

He was involved with semiconductor physics at Max-Planck-Institut für Festkörperforschung, Stuttgart, Germany, from 1996 to 1998 and with infrared sensors and systems at Acreo AB, Stockholm, Sweden, from 1998 to 2000. From 2000 to 2004, he was a Technical Consultant and Head of Research with Racomna AB, Uppsala, Sweden, where he worked with PA linearization and with "smart" materials for microwave applications. 2004-2006 he was a university lecturer at University of Gävle, Sweden. 2006-2011 he was a senior sensor engineer at Westerngeco, Oslo Norway, where he worked with signal processing and seismic sensors. In 2011 he became a professor in electronics at University of Gävle. He has been an Associate Professor with Uppsala University since 2000. He has authored or coauthored over 45 peer-reviewed papers and holds eight patents. His current research interests are RF measurement techniques, and linearization of nonlinear RF circuits and systems.